Cell Reports
Physical Science

CellPress
OPEN ACCESS

Article

Rational design of cooperative chelating sites on covalent organic frameworks for highly selective uranium extraction from seawater

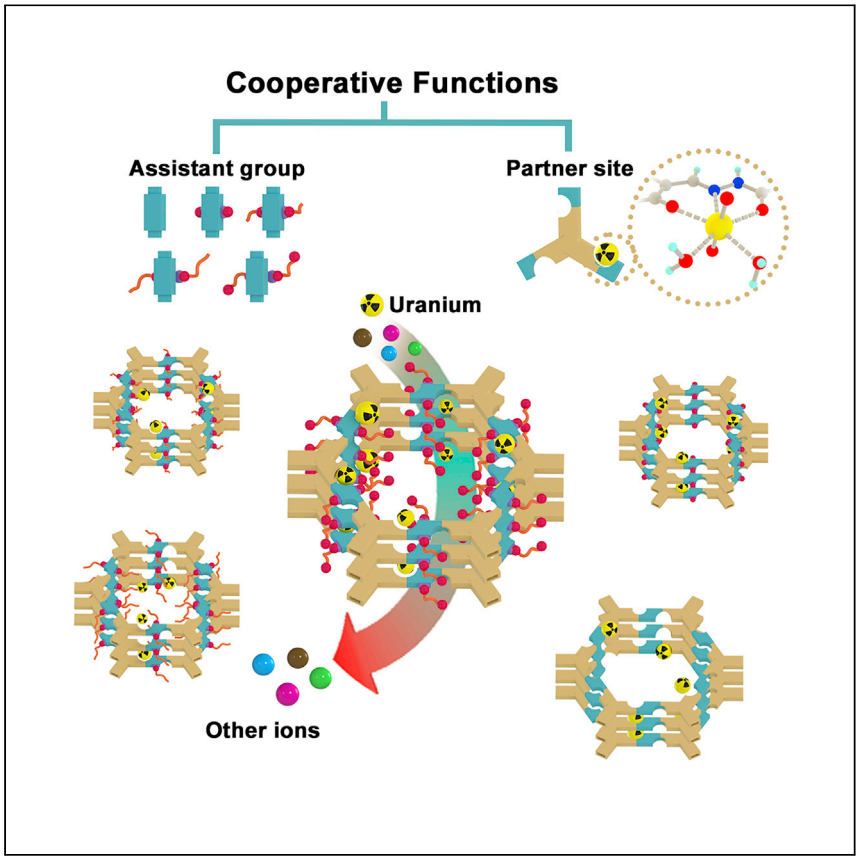

Xie et al. prepare covalent organic frameworks containing hydrazine-carbonyl groups and hydrazine-based linkers supporting assistant groups and applied them to uranium extraction from seawater. The presence of hydroxypropoxy assistant groups in the pores of the COFs is found to greatly enhance uranium adsorption, resulting in uranium selectivity, fast adsorption kinetics, and high uptake capacity.

Yinghui Xie, You Wu, Xiaolu Liu, ..., Xiangke Wang, Hui Yang, Shengqian Ma

h.yang@ncepu.edu.cn

Highlights

A series of COFs with hydrazine-carbonyl sites and assistant groups are synthesized

Hydrazine-carbonyl sites and hydroxypropoxy groups synergistically enhance UO_2^{2+} uptake

COF-R_5 shows a high UO_2^{2+} uptake capacity of 0.76/mg/g/d in natural seawater

COF-R_5 shows excellent selectivity for UO_2^{2+} versus other metal ions in seawater

Xie et al., Cell Reports Physical Science 4, 101220
January 18, 2023
https://doi.org/10.1016/j.xcrp.2022.101220

Cell Reports
Physical Science

CellPress
OPEN ACCESS

Article

Rational design of cooperative chelating sites on covalent organic frameworks for highly selective uranium extraction from seawater

Yinghui Xie,[1] You Wu,[1] Xiaolu Liu,[1] Mengjie Hao,[1] Zhongshan Chen,[1] Geoffrey I.N. Waterhouse,[2] Xiangke Wang,[1] Hui Yang,[1,4,*] and Shengqian Ma[3]

SUMMARY

Amidoxime-functionalized adsorbents have been pursued for uranium extraction from seawater, though competitive adsorption of vanadium and copper ions remains an issue. Herein, we report the successful design of a family of covalent organic framework (COF) adsorbents adopting an alternative chelating strategy for uranium binding comprising hydrazine-carbonyl sites with assistant groups for enhanced uranium uptake. A COF possessing hydroxypropoxy assistant groups (denoted as COF-R_5) showed exceptional selectivity for uranium over vanadium and other metal ions, resulting in a fast uranium adsorption kinetics and high uptake capacity of 11.3 mg/g with a distribution coefficient over 9.2 × 10^5 mL/g in seawater, which exceeded most COFs previously reported in the literature. Mechanism studies revealed that hydroxypropoxy groups enhanced the binding of UO_2^{2+} at the COF's hydrazine-carbonyl sites through hydrogen bonding interactions and charge stabilization effects, thus boosting the overall uranium affinity and adsorption capacity. Results validate the developed "uranium nanotraps" strategy for potential large-scale uranium extraction.

INTRODUCTION

The use of enriched uranium in nuclear fission reactors allows sustainable electricity generation with negligible carbon dioxide emissions. Thus, nuclear energy is expected to play an important support role in global efforts to decarbonize the energy sector. ^{235}U is an important nuclear fuel.[1–3] It is sourced from uranium ore and purified through chemical processing (enrichment, which removes other uranium isotopes including the more abundant ^{238}U). However, the limited terrestrial resources of uranium ore cannot satisfy the projected long-term needs of the nuclear energy industry. Therefore, researchers are now beginning to explore technologies that allow uranium extraction from seawater, which contains more than 1,000 times the amount of uranium as uranium ores.[4,5] The challenges of uranium extraction from seawater include the low uranium concentration (~3.3 ppb), high ionic strength, multitude of other metal and non-metal ions, and marine microorganisms. To address these challenges, efficient extraction technologies with fast kinetics and a large uranium uptake capacity are needed that can operate under ambient conditions.[6] Among the techniques currently being pursued for uranium mining from seawater, adsorptive extraction processes using solid porous adsorbents are the most prominent. Adsorbents such as nanofibers,[7,8] carbons and their composites,[9–12] hydrogels,[13] biomass-based materials,[14–16] hydrogen-bonded organic frameworks,[17] and metal-organic frameworks[18–25] have previously been applied

[1]College of Environmental Science and Engineering, North China Electric Power University, Beijing 102206, P.R. China

[2]School of Chemical Sciences, The University of Auckland, Auckland 1142, New Zealand

[3]Department of Chemistry, University of North Texas, Denton, TX 76201, USA

[4]Lead contact

*Correspondence: h.yang@ncepu.edu.cn

https://doi.org/10.1016/j.xcrp.2022.101220

for uranium extraction from seawater; however, they are not satisfactory due to one or more of the following limitations: slow adsorption kinetics, low adsorption capacities, or poor antibiofouling abilities.[26,27] Porous organic polymers (POPs) and porous aromatic frameworks (PAFs) are promising candidates,[28–38] but their performance is hampered by their disordered structures, which leads to blocking of uranium chelating sites.

Covalent organic frameworks (COFs) have found a niche as adsorbents for uranium extraction from seawater (and wastewater).[39–46] Among COF-based adsorbents, amidoxime-functionalized COFs have been the most widely studied because of the strong interaction between the amidoxime group and uranyl ions, thus enabling high adsorption capacities and fast kinetics.[47,48] However, the amidoxime group also shows modest affinities for vanadium and copper ions in natural seawater, reducing the uranium extraction efficiency and capacity.[38,48–50] The design of COF adsorbents with high selectivity toward uranium compared with vanadium and copper ions is essential for practical uranium extraction from seawater, with other design considerations including cost, non-toxicity, robustness, and recyclability.

Incorporating assistant groups into the pores of COF-based adsorbents is a promising strategy for fine-tuning the metal-binding affinity through modulating local chemical environments (e.g., uranium-binding sites), thus potentially offering a pathway for improved uranium extraction performance. In a notable recent contribution, it was shown that the introduction of amino ($–NH_2$) assistant groups into POPs could enhance the interaction between amidoxime chelating sites and uranyl ions, thereby boosting uranium uptake.[35] This work demonstrated that modifying the adsorption pocket of porous materials with metal-binding aides can enhance the metal-binding strength, thus enabling more specific binding of target metal ions under highly competitive ion adsorption conditions. Combining different functionalities in COF materials, such as chelating sites for metal binding and binding assistants, is therefore a rational approach for selective uranium extraction from seawater.

Based on this rationale, a series of COF-based adsorbents with well-defined porosity, abundant metal chelating sites, and different assistant groups were synthesized to address the challenge of selective uranium extraction from seawater. The architecture of COFs contained hydrazine-carbonyl partner chelating sites and different assistant groups (R) synergistically serving as "uranium nanotraps." The design of the COFs, denoted herein as COF-R_x (x = 1 to 5), is depicted in Figure 1. The microenvironment around the hydrazine-carbonyl uranium-binding sites was regulated and programmed by introducing assistant groups on the organic linkers in the COF building units. The introduced assistant groups affected the interaction between the hydrazine-carbonyl chelating site and uranyl, thus tuning the affinity (Figure 1). Through detailed studies, it is shown that the COF-R_5 containing flexible hydroxypropoxy groups in the pores in close proximity to the hydrazine-carbonyl binding sites showed good antibiofouling activity and exceptional affinity toward uranyl ions (relative to vanadium and other common metal ions in seawater), making it one of the best uranium extractants from seawater reported to date. Theoretical calculations revealed that the hydroxypropoxy groups influenced hydrogen bonding interactions and exerted charge stabilization effects (electron-donating properties), accounting for the superior performance of COF-R_5 relative to the other COF-R_x analogs. Our work offers valuable new strategies for improving the binding affinity of specific metal ions in COF-based adsorbents.

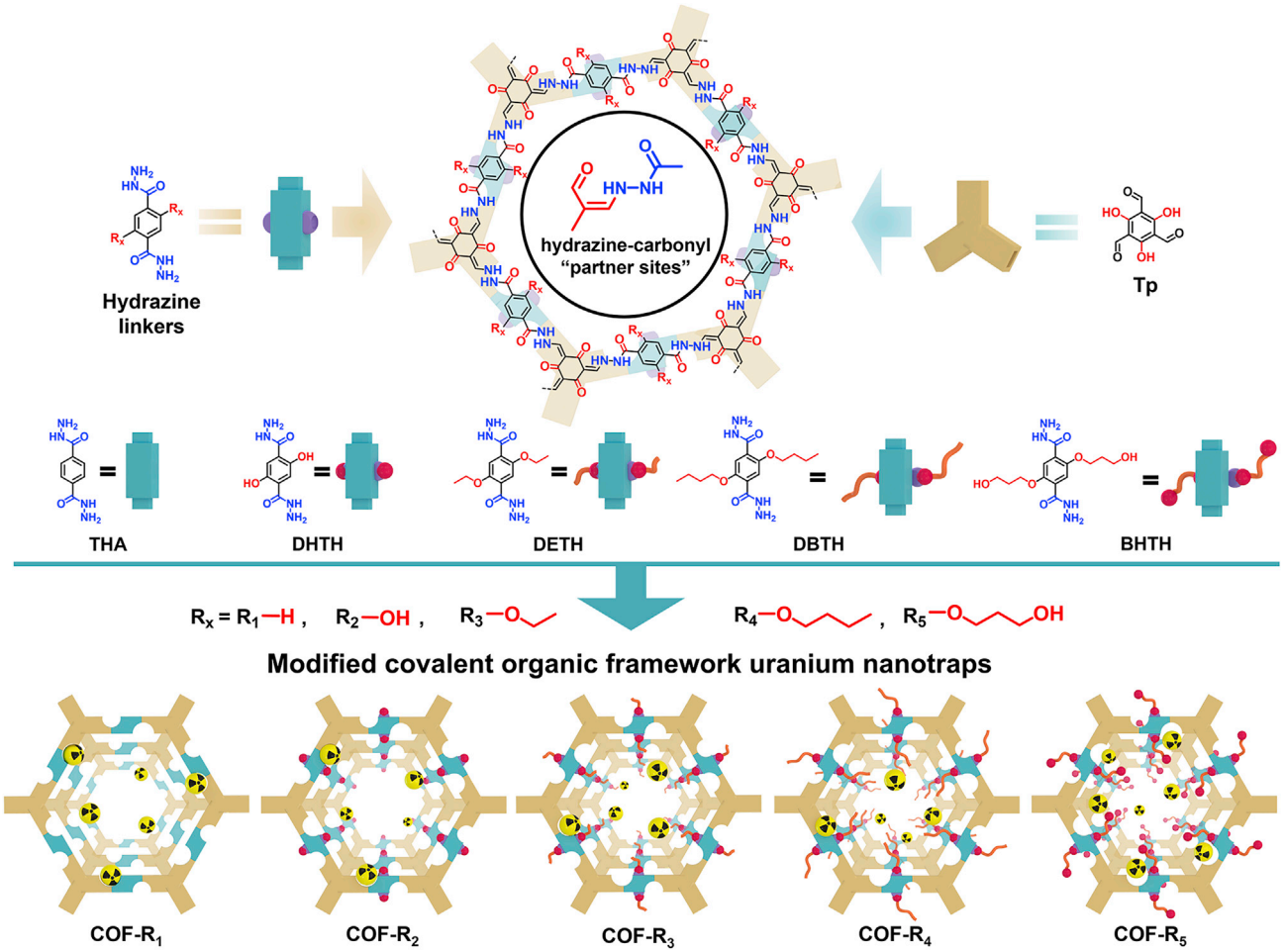

Figure 1. Bottom-up synthetic route to COF-R_x (through R_1 to R_5)

The developed COFs are equipped with hydrazine-carbonyl sites for uranyl chelation and assistant groups (R_x) that modulate the binding affinity (creating synergistic effects).

RESULTS

Synthesis and characterization of the COFs

COF-R_x supporting hydrazine-carbonyl partner sites and different functional groups (R_x) in the pores is illustrated in Figure 1. Here, R_x represents functional groups on the hydrazine linker. All designed COFs are hydrazone linked through hydrazone bonds to form 2D hexagonal mesoporous frameworks. Five different COFs, through COF-R_1 to COF-R_5, were synthesized by the condensation of 1,3,5-triformylphloroglucinol (TP) with terephthalohydrazide (THA); 2,5-bis((hydrazinyloxy)carbonyl)benzene-1,4-diol (DHTH); 2,5-diethoxyterephthalohydrazide (DETH); 2,5-dibutoxyterephthalohydrazide (DBTH); or 2,5-bis(3-hydroxypropoxy) terephthalohydrazide (BHTH), respectively, in a mixture of mesitylene and 1,4-dioxane with acetic acid as the catalyst at 120°C. We determined the structures of COF-R_1 to COF-R_5 from Fourier transform infrared (FTIR) spectroscopy, solid-state ^{13}C nuclear magnetic resonance (NMR) spectroscopy, powder X-ray diffraction (PXRD), and structural simulations in Materials Studio. The presence of the amide C=O stretching peak at 1,678 cm^{-1} and the –NH stretching peak at 3,261 cm^{-1} in the FTIR spectra of all the COFs confirmed the successful condensation reactions had proceeded in accordance with Figures S1 and S2. FTIR signals

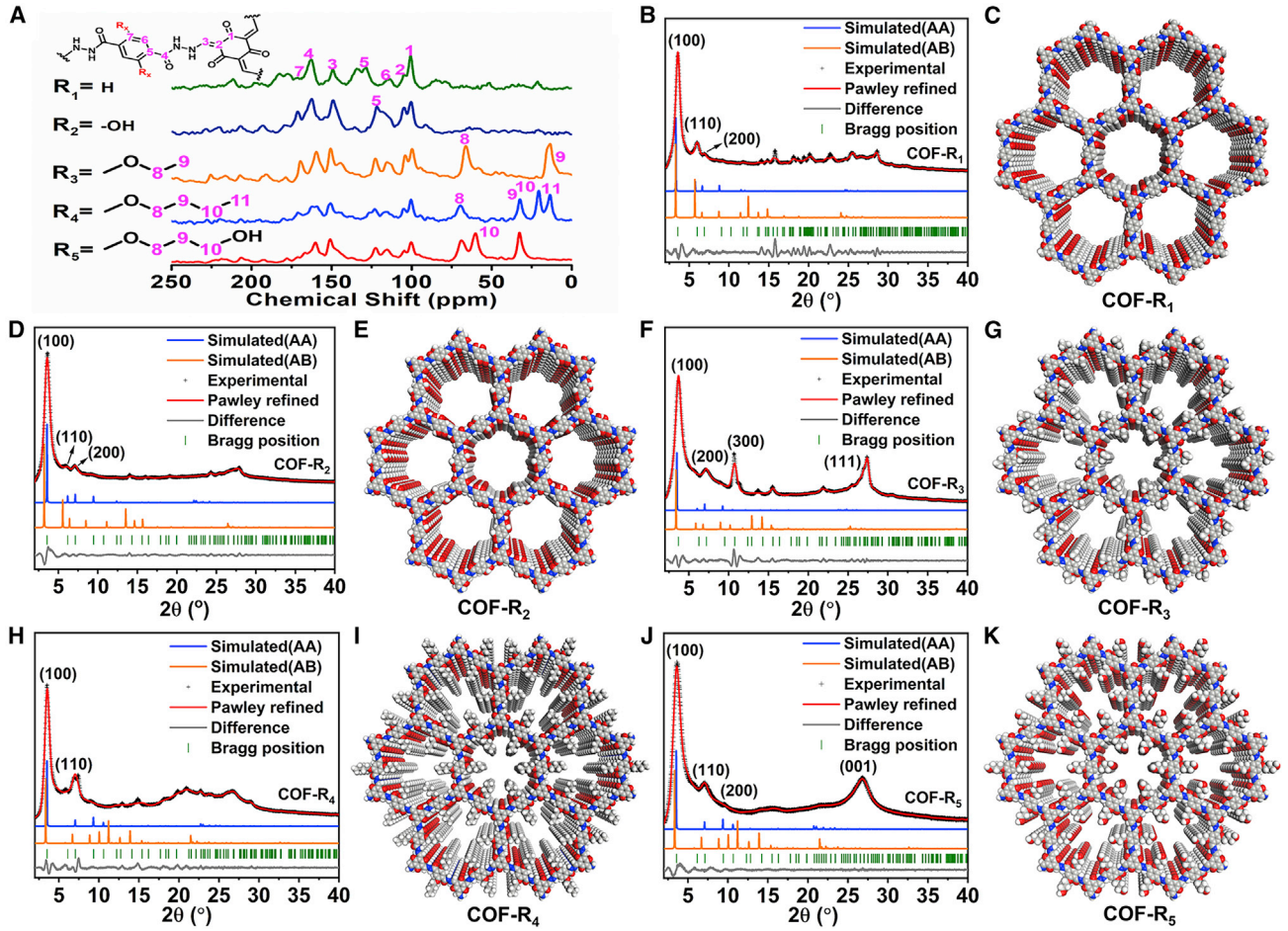

Figure 2. Structural characterization of COF-R_1 to COF-R_5

(A) Solid-state ^{13}C CP/MAS NMR spectra of COF-R_1, COF-R_2, COF-R_3, COF-R_4, and COF-R_5.

(B, D, F, H, and J) Experimental and simulated PXRD patterns of COF-R_1, COF-R_2, COF-R_3, COF-R_4, and COF-R_5.

(C, E, G, I, and K) Top view of the eclipsed AA stacking crystal structure of COF-R_1, COF-R_2, COF-R_3, COF-R_4, and COF-R_5. The C, N, O, and H atoms are represented by gray, blue, red, and white spheres, respectively.

from R_2 (hydroxyl), R_3 (ethoxy), R_4 (butoxy), and R_5 (hydroxypropoxy) functional groups in the hydrazine linkers were also seen in the corresponding COFs, suggesting that these functional groups were retained after being introduced into the COF frameworks. The solid-state ^{13}C NMR spectra of the COF-R_x samples further proved the starting materials had undergone condensation reactions to form COFs, evidenced by the appearance of C–NH and O=C–NH bonds at ~150 and ~162.5 ppm, respectively (Figure 2A). Further, the peaks around 100 ppm in the spectra of COF-R_x provided evidence for a newly formed ketone (Figure 2A).[51,52] The peaks observed in the region 10–70 ppm differed for each COF-R_x sample and thus could be used to "fingerprint" the individual COFs. These peaks are due to the ethoxy, butoxy, and hydroxypropoxy groups on the linkers, confirming the presence of additional assistant functional groups in the as-synthesized COFs (Figure 2A).

The crystalline structures of COF-R_x (x = 1 to 5) were determined by PXRD and Materials Studio theoretical simulations. The details are summarized in Tables S1–S5 and Figure 2. The experimental PXRD pattern of COF-R_1 showed peaks at 3.5°,

5.9°, and 6.9° corresponding to reflections from (100), (110), and (200) facets, respectively (Figure 2B). Next, Pawley refinement of a structural model based on the conformation COF-R_1 was performed against the experimental result using the Materials Studio software package.[53] The results revealed that COF-R_1 crystalized in a hexagonal P-6/M space group with unit cell parameters of a = b = 30.80 Å, c = 3.58 Å, $\alpha = \beta = 90°$, and $\gamma = 120°$, with R_P = 3.97% and R_{WP} = 5.96% (Table S1). The experimental data were good matches for the eclipsed (AA) stacking mode (Figure 2B). On the basis of these results, COF-R_1 possessed a 2D structure with honeycomb-like pores with a theoretical dynamic pore size of 2.61 nm (Figures 2C and S3). The interlayer distance is approximately 3.58 Å (Figure S3). The crystalline structures of COF-R_2 to COF-R_5 were also determined using experimental PXRD data, structure modeling, and Pawley refinements. The results are summarized in Tables S2–S5 and Figures 2D–2K and S4–S7. The unit cell parameters of COF-R_2 to COF-R_5 were found to be very similar to COF R_1, suggesting that all these COFs were isostructural porous neutral frameworks. FTIR and solid-state ^{13}C NMR spectra verified that the different functional groups were incorporated in each framework (Figures 2A, S1, and S2). Scanning electron microscopy (SEM) images showed the COFs to possess wire- and ribbon-like morphologies (Figures S11–S15).

Porosity, chemical and thermal stability, and hydrophilic properties

Thermogravimetric analysis (TGA) revealed that the COF-R_x materials were stable up to 300°C under an N_2 atmosphere (Figures S19–S23). Contact-angle measurements were carried out to determine the surface wettability of the COF-R_x samples. Measurements were performed on pressed pellets of each COF. As shown in Figure 3A, the contact angles of deionized water on the surface of COF-R_1, COF-R_2, COF-R_3, and COF-R_5 are 34°, 37°, 39°, and 37°, respectively, indicating good hydrophilicity. COF-R_4 showed relatively weak hydrophilicity with a contact angle around 85° due to the butoxy groups. The chemical stability of the COFs was next studied by immersing them in natural seawater and HNO_3 solutions. All COFs displayed excellent stability in HNO_3 (pH 1) and natural seawater over 24 h, as determined by both PXRD and FTIR results (Figures 3B–3E), suggesting excellent chemical stability.

The porosity of each COF was determined by nitrogen adsorption/desorption isotherms on fully activated samples at 77 K. The adsorption-desorption isotherms showed type IV (or type II) curves with Brunauer-Emmett-Teller (BET) surface areas ranging from 383.6 to 659.3 m^2/g (Figure 3F; Table S7). The calculated pore size distributions were in good general agreement with the observed pore sizes determined in the crystal simulations (Figure 3G). The total pore volumes ranged from 0.22 to 0.43 cm^3/g (Table S7). Since the ligand functional groups (assistant groups) are located in the large pores (1D channels), COF-R_5 with the largest functional groups showed the narrowest pore size among all COFs. The structural and chemical properties of the COF-R_x samples suggested suitability for uranium extraction from seawater or wastewater, an application that relies on adsorbents with good physical and chemical stability, fast adsorption kinetics, and a high adsorption capacity through abundant functional binding sites and porous structures for efficient mass transport. Here, we expected additional synergistic effects from the combination of hydrazine-carbonyl adsorption sites and assistant groups.

To validate the utility of using hydrazine-carbonyl partner adsorption sites together with assistant functional group synergistic effects (served as "uranium traps") for enhanced uranium adsorption, we also synthesized COF-6 by condensation of benzene-1,3,5-tricarbaldehyde (BTB) with BHTH at 120°C. The synthesis and characterization data for COF-6 are provided in the supplemental information

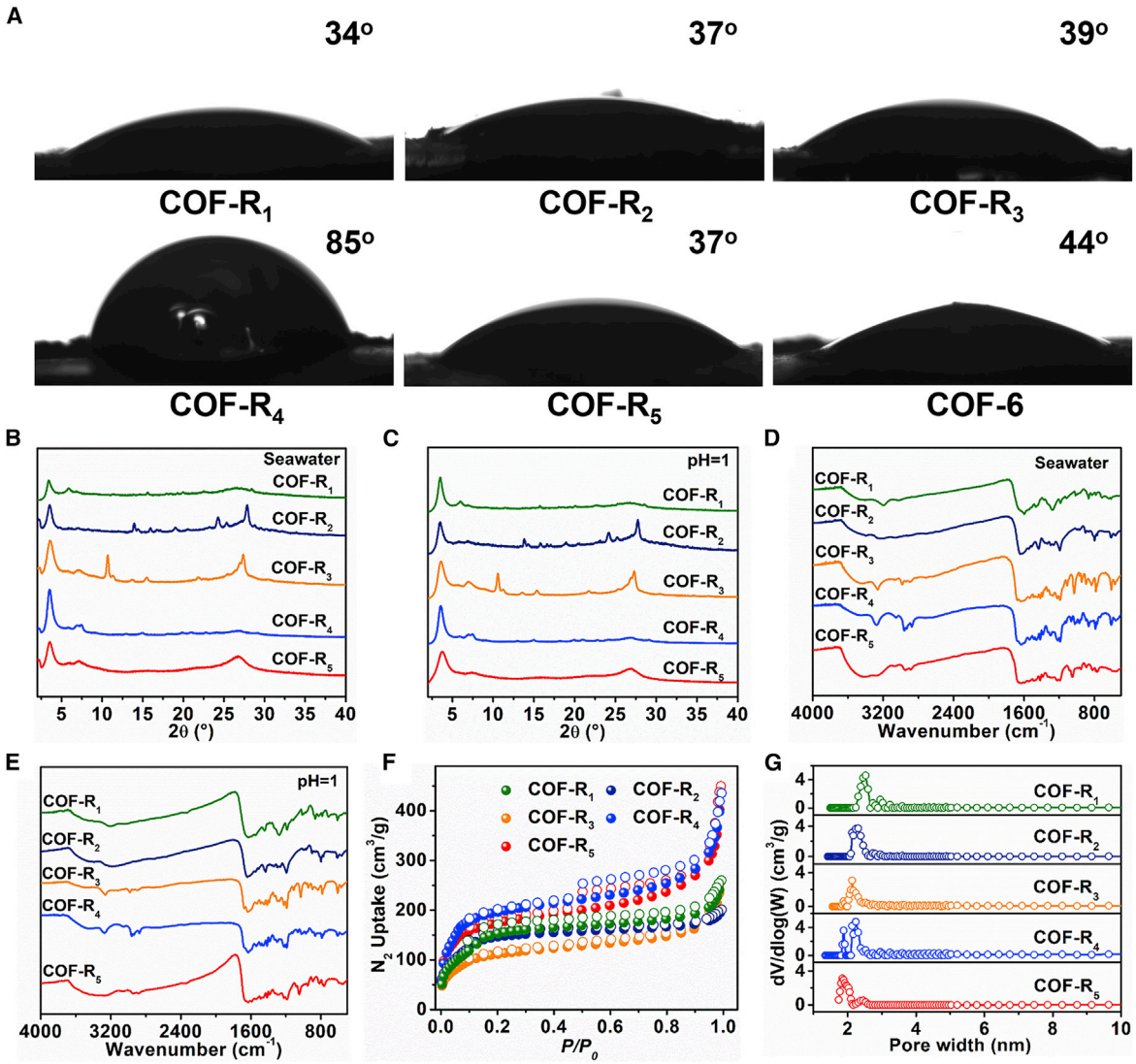

Figure 3. Hydrophilicity, stability and porosity of COFs

(A) Contact angles for deionized water on pressed pellets of COF-R_1, COF-R_2, COF-R_3, COF-R_4, COF-R_5, and COF-6.

(B and C) PXRD patterns of COF-R_1, COF-R_2, COF-R_3, COF-R_4, and COF-R_5 after treatment under different conditions.

(D and E) FTIR spectra of COF-R_1, COF-R_2, COF-R_3, COF-R_4, and COF-R_5 after treatment under different conditions.

(F and G) N_2 sorption isotherms and pore size distributions measured at 77 K for COF-R_1, COF-R_2, COF-R_3, COF-R_4, and COF-R_5.

(Figures S8–S10, S16–S18, and S24–S26; Tables S6 and S7).[54–56] COF-6 did not contain any hydrazine-carbonyl partner sites.

Uranium adsorption studies

To evaluate the uranium recovery ability, preliminary experiments were carried out in uranium-spiked seawater to determine the adsorption capacity and kinetics of the various COFs. To begin, the uranium adsorption abilities of all COFs were examined at initial pH values ranging from 2 to 9 (Figure 4A). COF-R_1 to COF-R_5 showed similar uptake capacities at initial pH values between 4 and 9, indicating the excellent adsorption properties under weak acidic, neutral, and weak alkaline environments. COF-6 offered much lower uptakes under the same conditions. An adsorbent-to-liquid ratio of 100 mg/L for each COF was used for subsequent studies.

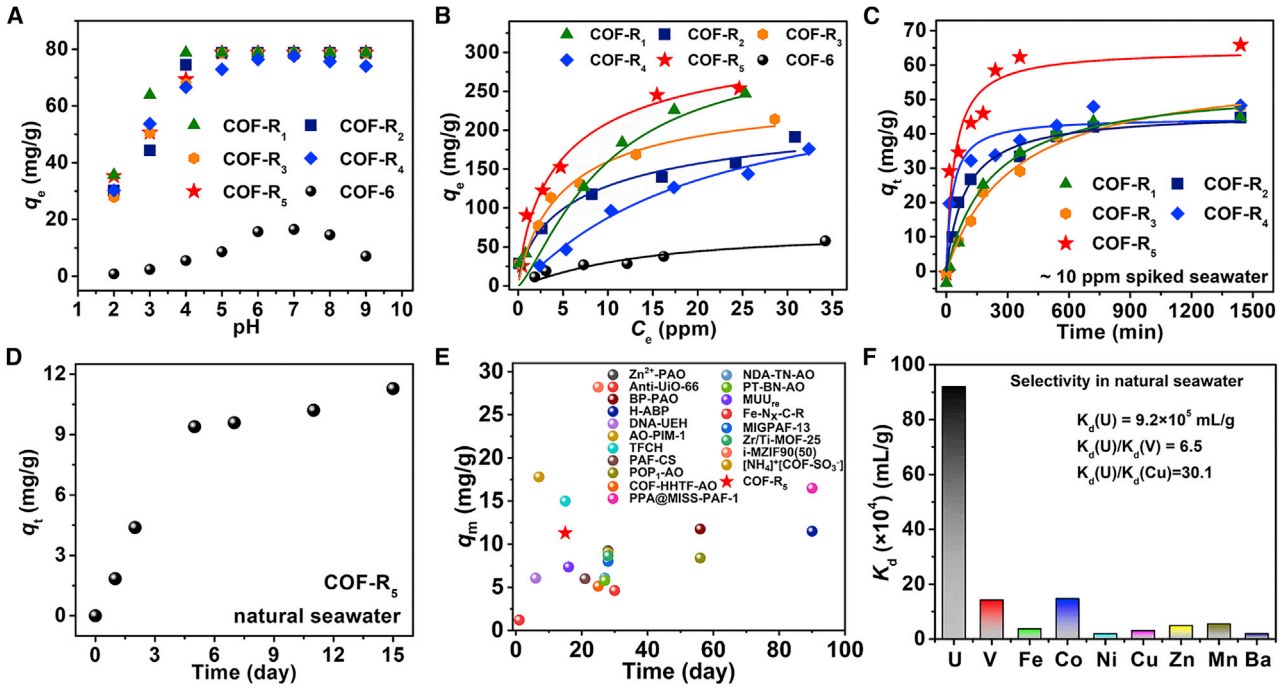

Figure 4. Uranium adsorption results

(A) Effect of initial pH on the removal of uranyl by different COF materials (in aqueous uranyl solution).

(B) Equilibrium adsorption isotherms for uranium adsorption on different COF materials in uranyl-spiked seawater at pH ~8 (uranium concentration from ~5 to ~50 ppm; fit lines for the Langmuir model are shown).

(C) Uranyl adsorption kinetics on different COF materials at an initial uranium concentration of ~10 ppm in uranyl-spiked seawater at pH ~8 (fit lines for the pseudo-second-order kinetic model are shown).

(D) Uranyl adsorption on COF-R_5 in natural seawater.

(E) Comparison of uranium uptake amount by COF-R_5 and other reported materials in natural seawater.

(F) Selectivity of COF-R_5 for different metals in natural seawater (15 days).

Next, equilibrium adsorption data were collected at pH ~8 (the pH of natural seawater) by varying the uranium concentration from ~5 to ~50 ppm (pH values were adjusted to ~8 by using Na_2CO_3). After 24 h, the experimental equilibrium adsorption capacities were 247, 191.4, 214.1, 176.2, and 253.7 mg/g for COF-R_1, COF-R_2, COF-R_3, COF-R_4, and COF-R_5, respectively (Figure 4B; Table S8). All the adsorption curves were fitted well by the Langmuir model, suggesting a monolayer adsorption process. To obtain adsorption kinetic isotherms, ~10 ppm uranium-spiked seawater solutions were treated with the COFs. COF-R_1, COF-R_2, COF-R_3, and COF-R_4 all demonstrated fast kinetics to reach their equilibrium uptakes, with the data following a pseudo-second-order kinetic model and suggesting that the rate-limiting step was a chemisorption process (Figure 4C). COF-R_5 possessed extremely rapid kinetics, achieving a removal equilibrium capacity of approximately 58.4 mg/g (>88.7%) within 240 min. In comparison, COF-6 showed much lower uptake capacity and slow kinetics under the similar conditions (Figures 4B and S27), which confirmed the key role of hydrazine-carbonyl partner sites in selective uranyl capture. COF-R_2, COF-R_3, and COF-R_4 produced roughly similar adsorption capacity and kinetics, while COF-R_5 showed the highest value of 253.7 mg/g with faster kinetics, suggesting that the hydroxypropoxy functional groups (as assistant groups) in COF-R_5 improved the uranium uptake performance. Following uranium uptake, COF-R_5 could be readily regenerated by elution with a Na_2CO_3 solution, with an adsorption capacity of 51 mg/g maintained over six cycles in ~10 ppm uranium-spiked seawater solutions (Figures S28 and S29). PXRD pattern and FTIR spectrum

of COF-R_5 confirmed excellent stability after cycling tests, suggesting the potential for long-term use (Figures S30 and S31).

Based on the promising uranium extraction performance of COF-R_5 in spiked seawater, we next carried out experiments to determine the ability of COF-R_5 to extract uranium from natural seawater. An adsorbent bed was prepared containing 10 mg COF-R_5 in a glass funnel (surrounded by sand above and cotton wool below), and then seawater circulated through the adsorbent bed and filtered for analysis at regular time intervals (Figure S32). The adsorption uptake capacities for COF-R_5 were determined to be 4.4, 9.4, and 11.3 mg/g after 2, 5, and 15 days, respectively (Figure 4D). The uranium extraction ability of COF-R_5 is on par or surpasses the best adsorbents previously reported, including high-performance amidoxime-based adsorbents (Figure 4E; Table S10).[13,14,19,29,45,47,49,57] Notably, COF-R_5 presents a high distribution coefficient (K_d) of 9.2×10^5 mL/g in capturing trace uranyl, indicating a strong affinity toward uranyl ions under high ionic strength conditions. Such high K_d values have rarely been reported in natural seawater. As is well known, amidoxime-functionalized adsorbents suffer from the competitive adsorption of vanadium present in seawater.[10,38,48–50] Comparison of the K_d values for uranium/vanadium and uranium/copper revealed that COF-R_5 showed 6.5 and 30.1 times higher uptake of uranium over vanadium and copper (15 days), respectively, indicating the exceedingly high U(VI)/V(V) and U(VI)/Cu(II) selectivity in natural seawater (Figure 4F). COF-R_5 also showed excellent selectivity for uranium against other metal ions under high ionic strength conditions. On the basis of the above results, we hypothesized that the high adsorption capacities, rapid uranium uptake kinetics, and excellent uranium selectivity over other metals demonstrated by COF-R_5 could be attributed to synergistic effects arising from the hydrazine-carbonyl partner adsorption sites and hydroxypropoxy assistant groups, which optimized the uranium binding affinity. Moreover, the 1D channels in COF-R_5 allowed rapid diffusion of uranyl ions in the adsorbent, which also acted to ensure fast uranium extraction performance. Adsorption mechanism studies are described below.

Uranium extraction mechanism studies

The high uranium extraction capacities and selectivity of COF-R_5 motivated an in-depth study of the adsorption interactions between hydrazine-carbonyl groups and uranyl, as well as the synergistic effects from the assistant groups. In particular, the addition of hydroxypropoxy functional groups in the pores of COF-R_5 improved the uranium adsorption performance, leading to the fast kinetics, good selectivity, and high capacities. In this regard, we first performed X-ray photoelectron spectroscopy (XPS) and X-ray absorption spectroscopy (XAS) measurements on COFs after uranium uptake to verify the local coordination and oxidation state of adsorbed uranyl. XPS spectra revealed that all COFs bind uranyl in a similar fashion in the form of U(VI) (Figures S33 and S34). Uranium L_{III}-edge X-ray absorption near-edge structure (XANES) analyses of UO_2^{2+}/COF-R_1 and UO_2^{2+}/COF-R_5 afforded spectra similar to the $UO_2(NO_3)_2 \cdot 6H_2O$ reference, which provided further confirmation for adsorbed U(VI) (Figure 5A). FT extended X-ray absorption fine structure (FT-EXAFS) analyses at the uranium L_{III} edge for UO_2^{2+}/COF-R_1 and UO_2^{2+}/COF-R_5 (Figure 5B) revealed two axial U=O bonds and two planar coordinated H_2O molecules in the first and second uranium coordination spheres, typical for uranyl ions. Further, the peak around 2.0 Å in R space is assigned to U–O and U–N bonds formed between hydrazine-carbonyl groups and uranyl. Fitting the scattering path suggested a local uranium environment containing two H_2O molecules, two oxygen atoms, and one nitrogen from hydrazine-carbonyl sites, confirming the predicted binding mode for COF-R_1 and COF-R_5 (Figures 5C and 5D; Table S11). EXAFS wavelet transform (WT) analysis

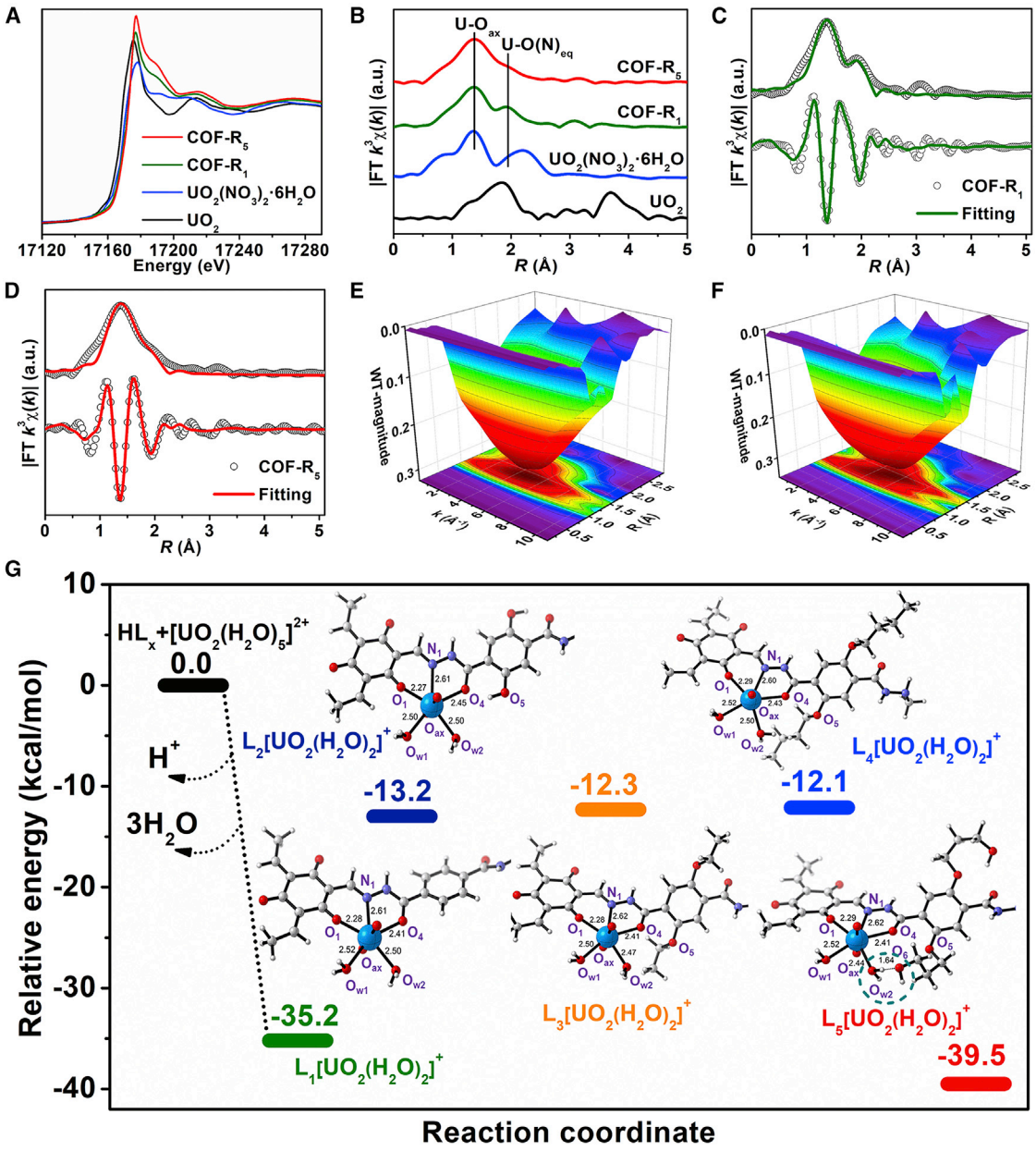

Figure 5. Uranium coordination and binding mechanism studies

(A) Uranium L_{III}-edge XANES spectra for COF-R_1 and COF-R_5 after uranium extraction studies. Data for UO_2 and $UO_2(NO_3)_2{\cdot}6H_2O$ are provided for comparison.

(B) FT k^3-weighted $\chi(k)$ function EXAFS spectra for COF-R_1 and COF-R_5 after uranium extraction studies. The reference data for $UO_2(NO_3)_2{\cdot}6H_2O$ in (A) and (B) were taken from our previous work.[10]

(C and D) EXAFS fitting curves for COF-R_1 and COF-R_5 after uranium extraction.

(E and F) WT contour plots for COF-R_1 and COF-R_5 after uranium extraction.

(G) Structural models of COF-R_1, COF-R_2, COF-R_3, COF-R_4, and COF-R_5 interacting with uranyl and binding free energies (kcal/mol) from DFT calculations. The C, N, O, U, and H atoms are represented by gray, violet, red, blue, and white spheres, respectively.

was further carried out to obtain additional information about the uranium coordination environment. Figures 5E, 5F, and S35 show the WT contour plots of COF-R_1, COF-R_5, UO_2, and $UO_2(NO_3)_2{\cdot}6H_2O$. After uranyl adsorption, COF-R_1 and COF-R_5 showed a single mixed scattering path signal involving U–O(N) bonds

with a maximum located at ~4.5 $Å^{-1}$ in k space and ~1.4 Å in R space, again clearly indicating the formation of U–O and U–N bonds.

Density functional theory (DFT) calculations were next conducted to calculate the uranyl adsorption energy, thereby pinpointing the respective roles of the assistant functional groups and hydrazine-carbonyl uranium chelating affinity sites in uranium uptake by the different COFs (i.e., COF-R_1 to COF-R_5). The Stuttgart/Dresden ECP (SDD ECP) basis set was used for uranium atoms, and 6-31G(d) was employed for other atoms for geometry optimization before performing the calculations.[58–64] In the modeling process, a condensed COF unit, including one hydrazine linker, one Tp molecule, and one uranyl, was employed as the full-scale model based on the XAS results (Figure 5G). The free energies of uranyl binding with COF-R_x (x = 1 to 5) were calculated and compared in Figure 5G. The calculated binding energies for UO_2^{2+}/COF-R_1; UO_2^{2+}/COF-R_2; UO_2^{2+}/COF-R_3; UO_2^{2+}/COF-R_4; and UO_2^{2+}/COF-R_5, were −35.2, −13.2, −12.3, −12.1, and −39.5 kcal/mol, respectively. This indicated that the uranyl binding affinity followed the order $R_5 > R_1 > R_2 \approx R_3 \approx R_4$. In addition to coordinative binding of uranyl ions at the hydrazine-carbonyl partner sites in COF-R_5, the hydroxypropoxy groups also served as hydrogen bond acceptor, showing strong second-sphere hydrogen bonding interaction with coordinated H_2O molecules of the hydrated uranyl ions, thus further improving the binding affinity (Figure 5G). In comparison, the hydroxyl linker groups in COF-R_2 resulted in strong hydrogen bonding interactions with the oxygen atoms of hydrazine groups, reducing the negative electrical density around uranium atoms and thus weakening the affinities. The ethoxy and butoxy groups in COF-R_3 and COF-R_4 resulted in electronic repulsion of uranyl, resulting in a significant decrease in the binding free energies. Based on the calculation results, the uranyl preferentially adsorbs on the hydrazine-carbonyl partner sites, with the hydroxypropoxy groups in COF-R_5 enhancing the binding energy due to the synergistic hydrogen bonding interactions. The theoretical calculations are thus in excellent accord with our experimental findings, further confirming the efficient and selective uranium adsorption properties of COF-R_5.

Antibiofouling activity of COF-R_5

Many adsorbents are quickly passivated by biofouling when used in seawater, reducing the adsorption capabilities. Accordingly, adsorbents should intrinsically inhibit biofouling to overcome this issue. We carried out antibacterial studies on COF-R_5 by measuring the ability of this COF to inhibit marine bacteria in seawater. As shown in Figures 6A, 6B, and 6E, an inhibition rate of 44% was achieved for COF-R_5 in the dark. Compared with dark conditions, the inhibition rate reached 98% under visible light conditions, suggesting that the COF possessed photocatalytic properties sufficient to prevent biofouling and biofilm formation on the surface of the adsorbent (Figures 6C–6E; Table S12). These results suggest that COF-R_5 would offer a high uranium adsorption capacity and fast kinetics in seawater while also offering excellent durability and recyclability. Results demonstrate that COF-R_5 offers many desirable characteristics for practical uranium extraction from seawater.

DISCUSSION

The aforementioned experimental and theoretical investigations validated the synthetic strategies adopted in this work for producing highly efficient uranium adsorbents beyond traditional amidoxime-functionalized materials. High binding affinities for uranyl ions were realized through cooperation of hydrazine-carbonyl uranyl

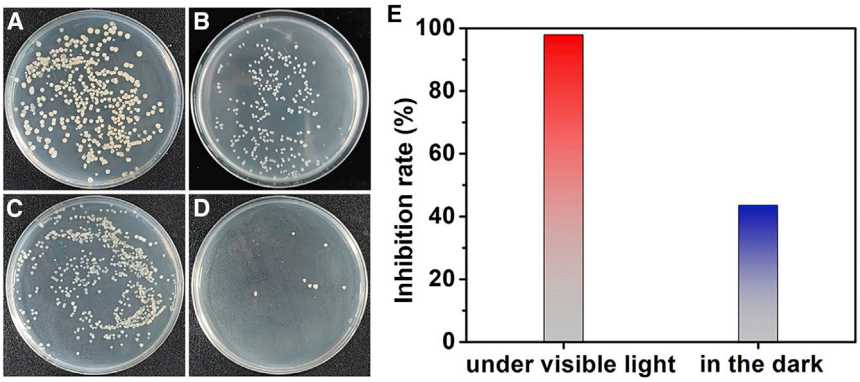

Figure 6. Marine antibiofouling experimental results

(A and C) Photographs of marine bacteria colonies grown in the dark and under visible light conditions without any adsorbent.

(B and D) Photographs of marine bacteria colonies incubated with COF-R_5 in the dark and under visible light illumination.

(E) Inhibition rates of marine bacteria by COF-R_5 under dark and light conditions.

selective recognition motifs (as newly developed uranium traps) and the fine-tuning of uranyl binding using assistant groups in the COF linkers. The COF with the optimized uranyl-binding sites (COF-R_5) delivered fast uranium adsorption kinetics, the strongest uranyl binding affinity, a high adsorption capacity, high uranium/vanadium selectivity, and good antibiofouling activity, ranking as one of the best all-around molecular chelators reported to date for uranyl extraction from seawater. This work draws attention to the roles of assistant groups in the pores of COFs for enhancing metal ion uptake, with the hydrogen bonding and electron donating capabilities of hydroxypropoxy groups in COF-R_5 being highly beneficial for optimizing uranyl uptake. In addition, we estimated the cost of synthesizing COF-R_5 to be ~$1.73 USD/g, suggesting the economic feasibility of the adsorbent. Moreover, the cost for uranium extraction using COF-R_5 was estimated to be ~$28 USD/g (based on cycling use of adsorbent). We anticipate that our proof-of-concept strategy will encourage other researchers to explore new strategies for the selective adsorption of uranium (moving beyond traditional amidoxime strategies) and other metal ions from seawater and other systems (such as actinide-chemistry-related areas).[65–67]

In summary, a series of COF materials with hydrazine-carbonyl groups were successfully synthesized and structurally characterized. To improve the affinity for uranyl ion capture, assistant functional groups were introduced in the COF pores. Detailed experimental and computational studies showed that COF-R_5, possessing hydroxypropoxy groups, delivered a high uranyl affinity, good antibiofouling activity, fast adsorption kinetics, and high uranium uptake capacity of 11.3 mg/g over 15 days (~0.76 mg/g/day) in natural seawater, ranking it as one of the best uranium adsorbents reported to date. XAS and DFT theoretical calculations results revealed that the hydrazine-carbonyl partner sites in the COF pore framework worked synergistically with the hydroxypropoxy assistant groups to coordinate uranyl ions (the latter involving hydrogen bonding between the hydroxypropoxy groups and a water molecule bound to uranium atoms in uranyl). Our successful COF design strategy shows that engineering novel uranium-binding sites and further fine-tuning uranyl affinities through secondary assistant groups allow the synthesis of low-cost adsorbents for uranium extraction from seawater, as well as other systems including nuclear waste, contaminated water, and in environmental remediation.

EXPERIMENTAL PROCEDURES

Resource availability

Lead contact

Further information and requests for resources and reagents should be directed to and will be fulfilled by the lead contact, Hui Yang (h.yang@ncepu.edu.cn).

Materials availability

This study did not generate new unique reagents.

Data and code availability

This article includes all datasets generated or analyzed in this study.

Synthesis of COF-R_1

TP (21 mg) and THA (29.2 mg) were dissolved in a mixed solvent solution containing mesitylene (1.5 mL)/1,4-dioxane (0.5 mL)/acetic acid (6 M, 0.2 mL) in a 5 mL glass tube. Next, the mixture was sonicated and frozen in a liquid nitrogen bath and sealed with a gas torch. The tube was then heated at 120°C for 72 h, after which the product was collected by filtration and washed several times with acetone and ethanol, yielding COF-R_1.

Synthesis of COF-R_2

DHTH (22.6 mg) and TP (21 mg) were dissolved in a mixed solvent solution containing mesitylene (1 mL)/1,4-dioxane (1 mL)/acetic acid (6 M, 0.2 mL) in a 5 mL glass tube. Next, the mixture was sonicated and frozen in a liquid nitrogen bath and sealed with a gas torch. The tube was then heated at 120°C for 72 h, after which the product was collected by filtration and washed several times with acetone and ethanol, yielding COF-R_2.

Synthesis of COF-R_3

DETH (28.2 mg) and TP (21 mg) were dissolved in a mixed solvent solution containing mesitylene (0.5 mL)/1,4-dioxane (1.5 mL)/acetic acid (6 M, 0.2 mL) in a 5 mL glass tube. Next, the mixture was sonicated and frozen in a liquid nitrogen bath and sealed with a gas torch. The tube was then heated at 120°C for 72 h, after which the product was collected by filtration and washed several times with acetone and ethanol, yielding COF-R_3.

Synthesis of COF-R_4

BDTH (33.8 mg) and TP (21 mg) were dissolved in a mixed solvent solution containing mesitylene (0.5 mL)/1,4-dioxane (1.5 mL)/acetic acid (6 M, 0.2 mL) in a 5 mL glass tube. Next, the mixture was sonicated and frozen in a liquid nitrogen bath and sealed with a gas torch. The tube was then heated at 120°C for 72 h, after which the product was collected by filtration and washed several times with acetone and ethanol, yielding COF-R_4.

Synthesis of COF-R_5

BHTH (34.2 mg) and TP (21 mg) were dissolved in a mixed solvent solution containing mesitylene (0.5 mL)/1,4-dioxane (1.5 mL)/acetic acid (6 M, 0.3 mL) in a 5 mL glass tube. Next, the mixture was sonicated and frozen in a liquid nitrogen bath and sealed with a gas torch. The tube was then heated at 120°C for 72 h, after which the product was collected by filtration and washed several times with acetone and ethanol, yielding COF-R_5

Synthesis of COF-6

BTB (16.2 mg) and BHTH (34.2 mg) were dissolved in a mixed solvent solution containing mesitylene (1 mL)/1,4-dioxane (1 mL)/acetic acid (6 M, 0.2 mL) in a 5 mL glass tube. Next, the mixture was sonicated and frozen in a liquid nitrogen bath and sealed with a gas torch. The tube was then heated at 120°C for 72 h, after which the product was collected by filtration and washed several times with acetone and ethanol, yielding COF-6.

SUPPLEMENTAL INFORMATION

Supplemental information can be found online at https://doi.org/10.1016/j.xcrp.2022.101220.

ACKNOWLEDGMENTS

We gratefully acknowledge funding support from the National Natural Science Foundation of China (grants U2167218, 22006036, and 22276054); the Science Challenge Project (TZ2016004); the Beijing Outstanding Young Scientist Program (H.Y., Z.C., and X.W.); and the Robert A. Welch Foundation (B−0027) (S.M.). G.I.N.W. is supported by a James Cook Research Fellowship from New Zealand Government funding, administered by the Royal Society Te Apārangi. We also acknowledge support from the BL 14W1 Beam line in Shanghai Synchrotron Radiation Facility (SSRF).

AUTHOR CONTRIBUTIONS

H.Y., X.W., and S.M. conceived and designed the research. Y.X., Y.W., X.L., M.H., and Z.C. performed the synthesis and characterization. Y.X. and Z.C. carried out the adsorption tests. H.Y., G.I.N.W., X.W., and S.M. wrote the manuscript. All authors contributed to the discussion and gave approval to the final version of the manuscript.

DECLARATION OF INTERESTS

The authors declare no competing interests.

Received: October 17, 2022
Revised: November 21, 2022
Accepted: December 9, 2022
Published: January 3, 2023

REFERENCES

1. Taylor, R. (2016). Reaction: a role for actinide chemists. Chem *1*, 662–663.
2. Deutch, J. (2020). Is net zero carbon 2050 possible? Joule *4*, 2237–2240.
3. Gilbert, A.Q., and Bazilian, M.D. (2020). Can distributed nuclear power address energy resilience and energy poverty? Joule *4*, 1839–1843.
4. Wiechert, A.I., Yiacoumi, S., and Tsouris, C. (2021). The ocean's nuclear energy reserve. Nat. Sustain. *5*, 13–14.
5. Dai, S. (2021). Catalyst: challenges in development of adsorbents for recovery of uranium from seawater. Chem *7*, 537–539.
6. Abney, C.W., Mayes, R.T., Saito, T., and Dai, S. (2017). Materials for the recovery of uranium from seawater. Chem. Rev. *117*, 13935–14013.
7. Xu, X., Yue, Y., Cai, D., Song, J., Han, C., Liu, Z., Wang, D., Xiao, J., and Wu, H. (2020). Aqueous solution blow spinning of seawater-stable polyamidoxime nanofibers from water-soluble precursor for uranium extraction from seawater. Small Methods *4*, 2000558.
8. Brown, S., Yue, Y., Kuo, L.-J., Mehio, N., Li, M., Gill, G., Tsouris, C., Mayes, R.T., Saito, T., and Dai, S. (2016). Uranium adsorbent fibers prepared by atom-transfer radical polymerization (ATRP) from poly(vinyl chloride)-co-chlorinated poly(vinyl chloride) (PVC-co-CPVC) fiber. Ind. Eng. Chem. Res. *55*, 4139–4148.
9. Wang, Z., Ma, R., Meng, Q., Yang, Y., Ma, X., Ruan, X., Yuan, Y., and Zhu, G. (2021). Constructing uranyl-specific nanofluidic channels for unipolar ionic transport to realize ultrafast uranium extraction. J. Am. Chem. Soc. *143*, 14523–14529.
10. Yang, H., Liu, X., Hao, M., Xie, Y., Wang, X., Tian, H., Waterhouse, G.I.N., Kruger, P.E., Telfer, S.G., and Ma, S. (2021). Functionalized iron-nitrogen-carbon electrocatalyst provides a reversible electron transfer platform for efficient uranium extraction from seawater. Adv. Mater. *33*, 2106621.
11. Yue, Y., Sun, X., Mayes, R.T., Kim, J., Fulvio, P.F., Qiao, Z., Brown, S., Tsouris, C., Oyola, Y., and Dai, S. (2013). Polymer-coated nanoporous carbons for trace seawater uranium adsorption. Sci. China Chem. *56*, 1510–1515.
12. Li, N., Yang, L., Wang, D., Tang, C., Deng, W., and Wang, Z. (2021). High-capacity amidoxime-functionalized beta-cyclodextrin/graphene aerogel for selective uranium capture. Environ. Sci. Technol. *55*, 9181–9188.
13. Yan, B., Ma, C., Gao, J., Yuan, Y., and Wang, N. (2020). An ion-crosslinked supramolecular

hydrogel for ultrahigh and fast uranium recovery from seawater. Adv. Mater. *32*, 1906615.

14. Yuan, Y., Liu, T., Xiao, J., Yu, Q., Feng, L., Niu, B., Feng, S., Zhang, J., and Wang, N. (2020). DNA nano-pocket for ultra-selective uranyl extraction from seawater. Nat. Commun. *11*, 5708.

15. Kou, S., Yang, Z., and Sun, F. (2017). Protein hydrogel microbeads for selective uranium mining from seawater. ACS Appl. Mater. Interfaces *9*, 2035–2039.

16. Yuan, Y., Yu, Q., Wen, J., Li, C., Guo, Z., Wang, X., et al. (2019). Ultrafast and highly selective uranium extraction from seawater by hydrogel-like spidroin-based protein fiber. Angew. Chem. Int. Ed. *58*, 11785–11790.

17. Kaushik, A., Marvaniya, K., Kulkarni, Y., Bhatt, D., Bhatt, J., Mane, M., Suresh, E., Tothadi, S., Patel, K., and Kushwaha, S. (2022). Large-area self-standing thin film of porous hydrogen-bonded organic framework for efficient uranium extraction from seawater. Chem *8*, 2749–2765.

18. Liu, W., Dai, X., Bai, Z., Wang, Y., Yang, Z., Zhang, L., Xu, L., Chen, L., Li, Y., Gui, D., et al. (2017). Highly sensitive and selective uranium detection in natural water systems using a luminescent mesoporous metal-organic framework equipped with abundant lewis basic sites: a combined batch, X-ray absorption spectroscopy, and first principles simulation investigation. Environ. Sci. Technol. *51*, 3911–3921.

19. Yu, Q., Yuan, Y., Wen, J., Zhao, X., Zhao, S., Wang, D., Li, C., Wang, X., and Wang, N. (2019). A universally applicable strategy for construction of anti-biofouling adsorbents for enhanced uranium recovery from seawater. Adv. Sci. *6*, 1900002.

20. Zhang, H., Liu, W., Li, A., Zhang, D., Li, X., Zhai, F., et al. (2019). Three mechanisms in one material: uranium capture by a polyoxometalate-organic framework through combined complexation, chemical reduction, and photocatalytic reduction. Angew. Chem. Int. Ed. *58*, 16110–16114.

21. Feng, L., Wang, H., Feng, T., Yan, B., Yu, Q., Zhang, J., et al. (2022). In situ synthesis of uranyl-imprinted nanocage for selective uranium recovery from seawater. Angew. Chem. Int. Ed. *61*, 82–86.

22. Chen, L., Bai, Z., Zhu, L., Zhang, L., Cai, Y., Li, Y., Liu, W., Wang, Y., Chen, L., Diwu, J., et al. (2017). Ultrafast and efficient extraction of uranium from seawater using an amidoxime appended metal-organic framework. ACS Appl. Mater. Interfaces *9*, 32446–32451.

23. Wu, H., Chi, F., Zhang, S., Wen, J., Xiong, J., and Hu, S. (2019). Control of pore chemistry in metal-organic frameworks for selective uranium extraction from seawater. Microporous Mesoporous Mater. *288*, 109567.

24. Liu, T., Tang, S., Wei, T., Chen, M., Xie, Z., Zhang, R., Liu, Y., and Wang, N. (2022). Defect-engineered metal-organic framework with enhanced photoreduction activity toward uranium extraction from seawater. Cell Rep. Phys. Sci. *3*, 100892.

25. Mollick, S., Saurabh, S., More, Y.D., Fajal, S., Shirolkar, M.M., Mandal, W., and Ghosh, S.K. (2022). Benchmark uranium extraction from seawater using an ionic macroporous metal–organic framework. Energy Environ. Sci. *15*, 3462–3469.

26. Gill, G.A., Kuo, L.-J., Janke, C.J., Park, J., Jeters, R.T., Bonheyo, G.T., Pan, H.-B., Wai, C., Khangaonkar, T., Bianucci, L., et al. (2016). The uranium from seawater program at the pacific northwest national laboratory: overview of marine testing, adsorbent characterization, adsorbent durability, adsorbent toxicity, and deployment studies. Ind. Eng. Chem. Res. *55*, 4264–4277.

27. Park, J., Gill, G.A., Strivens, J.E., Kuo, L.-J., Jeters, R.T., Avila, A., Wood, J.R., Schlafer, N.J., Janke, C.J., Miller, E.A., et al. (2016). Effect of biofouling on the performance of amidoxime-based polymeric uranium adsorbents. Ind. Eng. Chem. Res. *55*, 4328–4338.

28. Yuan, Y., Yang, Y., Ma, X., Meng, Q., Wang, L., Zhao, S., and Zhu, G. (2018). Molecularly imprinted porous aromatic frameworks and their composite components for selective extraction of uranium ions. Adv. Mater. *30*, 1706507.

29. Li, Z., Meng, Q., Yang, Y., Zou, X., Yuan, Y., and Zhu, G. (2020). Constructing amidoxime-modified porous adsorbents with open architecture for cost-effective and efficient uranium extraction. Chem. Sci. *11*, 4747–4752.

30. Song, Y., Zhu, C., Sun, Q., Aguila, B., Abney, C.W., Wojtas, L., and Ma, S. (2021). Nanospace decoration with uranyl-specific "Hooks" for selective uranium extraction from seawater with ultrahigh enrichment index. ACS Cent. Sci. *7*, 1650–1656.

31. Sun, Q., Song, Y., Aguila, B., Ivanov, A.S., Bryantsev, V.S., and Ma, S. (2021). Spatial engineering direct cooperativity between binding sites for uranium sequestration. Adv. Sci. *8*, 2001573.

32. Yang, L., Xiao, H., Qian, Y., Zhao, X., Kong, X.-Y., Liu, P., et al. (2022). Bioinspired hierarchical porous membrane for efficient uranium extraction from seawater. Nat. Sustain. *5*, 71–80.

33. Kuo, L.-J., Janke, C.J., Wood, J.R., Strivens, J.E., Das, S., Oyola, Y., Mayes, R.T., and Gill, G.A. (2015). Characterization and testing of amidoxime-based adsorbent materials to extract uranium from natural seawater. Ind. Eng. Chem. Res. *55*, 4285–4293.

34. Yue, Y., Mayes, R.T., Kim, J., Fulvio, P.F., Sun, X.G., Tsouris, C., et al. (2013). Seawater uranium sorbents: preparation from a mesoporous copolymer initiator by atom-transfer radical polymerization. Angew. Chem. Int. Ed. *52*, 13458–13462.

35. Sun, Q., Aguila, B., Perman, J., Ivanov, A.S., Bryantsev, V.S., Earl, L.D., Abney, C.W., Wojtas, L., and Ma, S. (2018). Bio-inspired nano-traps for uranium extraction from seawater and recovery from nuclear waste. Nat. Commun. *9*, 1644.

36. Yuan, Y., Meng, Q., Faheem, M., Yang, Y., Li, Z., Wang, Z., Deng, D., Sun, F., He, H., Huang, Y., et al. (2019). A molecular coordination template strategy for designing selective porous aromatic framework materials for uranyl capture. ACS Cent. Sci. *5*, 1432–1439.

37. Wang, Z., Meng, Q., Ma, R., Wang, Z., Yang, Y., Sha, H., Ma, X., Ruan, X., Zou, X., Yuan, Y., and Zhu, G. (2020). Constructing an ion pathway for uranium extraction from seawater. Chem *6*, 1683–1691.

38. Yuan, Y., Yu, Q., Cao, M., Feng, L., Feng, S., Liu, T., Feng, T., Yan, B., Guo, Z., and Wang, N. (2021). Selective extraction of uranium from seawater with biofouling-resistant polymeric peptide. Nat. Sustain. *4*, 708–714.

39. Zhang, S., Zhao, X., Li, B., Bai, C., Li, Y., Wang, L., Wen, R., Zhang, M., Ma, L., and Li, S. (2016). "Stereoscopic" 2D super-microporous phosphazene-based covalent organic framework: design, synthesis and selective sorption towards uranium at high acidic condition. J. Hazard Mater. *314*, 95–104.

40. Sun, Q., Aguila, B., Earl, L.D., Abney, C.W., Wojtas, L., Thallapally, P.K., and Ma, S. (2018). Covalent organic frameworks as a decorating platform for utilization and affinity enhancement of chelating sites for radionuclide sequestration. Adv. Mater. *30*, 1705479.

41. Wen, R., Li, Y., Zhang, M., Guo, X., Li, X., Li, X., Han, J., Hu, S., Tan, W., Ma, L., and Li, S. (2018). Graphene-synergized 2D covalent organic framework for adsorption: a mutual promotion strategy to achieve stabilization and functionalization simultaneously. J. Hazard Mater. *358*, 273–285.

42. Song, Y., Sun, Q., Aguila, B., and Ma, S. (2019). Opportunities of covalent organic frameworks for advanced applications. Adv. Sci. *6*, 1801410.

43. Geng, K., He, T., Liu, R., Dalapati, S., Tan, K.T., Li, Z., Tao, S., Gong, Y., Jiang, Q., and Jiang, D. (2020). Covalent organic frameworks: design, synthesis, and functions. Chem. Rev. *120*, 8814–8933.

44. Li, Y., Guo, X., Li, X., Zhang, M., Jia, Z., Deng, Y., et al. (2020). Redox-active two-dimensional covalent organic frameworks (COFs) for selective reductive separation of valence-variable, redox-sensitive and long-lived radionuclides. Angew. Chem. Int. Ed. *59*, 4168–4175.

45. Cheng, G., Zhang, A., Zhao, Z., Chai, Z., Hu, B., Han, B., Ai, Y., and Wang, X. (2021). Extremely stable amidoxime functionalized covalent organic frameworks for uranium extraction from seawater with high efficiency and selectivity. Sci. Bull. *66*, 1994–2001.

46. Xiong, X.H., Yu, Z.W., Gong, L.L., Tao, Y., Gao, Z., Wang, L., Yin, W.H., Yang, L.X., and Luo, F. (2019). Ammoniating covalent organic framework (COF) for high-performance and selective extraction of toxic and radioactive uranium ions. Adv. Sci. *6*, 1900547.

47. Cui, W.-R., Zhang, C.-R., Xu, R.-H., Chen, X.-R., Yan, R.-H., Jiang, W., Liang, R.-P., and Qiu, J.-D. (2020). High-efficiency photoenhanced extraction of uranium from natural seawater by olefin-linked covalent organic frameworks. ACS EST. Water *1*, 440–448.

48. Cui, W.-R., Li, F.-F., Xu, R.-H., Zhang, C.-R., Chen, X.-R., Yan, R.-H., et al. (2020). Regenerable covalent organic frameworks for photo-enhanced uranium adsorption from

seawater. Angew. Chem. Int. Ed. *59*, 17684–17690.

49. Xu, X., Zhang, H., Ao, J., Xu, L., Liu, X., Guo, X., Li, J., Zhang, L., Li, Q., Zhao, X., et al. (2019). 3D hierarchical porous amidoxime fibers speed up uranium extraction from seawater. Energy Environ. Sci. *12*, 1979–1988.

50. Wang, D., Song, J., Lin, S., Wen, J., Ma, C., Yuan, Y., Lei, M., Wang, X., Wang, N., and Wu, H. (2019). A marine-inspired hybrid sponge for highly efficient uranium extraction from seawater. Adv. Funct. Mater. *29*, 1970219.

51. Kandambeth, S., Mallick, A., Lukose, B., Mane, M.V., Heine, T., and Banerjee, R. (2012). Construction of crystalline 2D covalent organic frameworks with remarkable chemical (acid/base) stability via a combined reversible and irreversible route. J. Am. Chem. Soc. *134*, 19524–19527.

52. Biswal, B.P., Chandra, S., Kandambeth, S., Lukose, B., Heine, T., and Banerjee, R. (2013). Mechanochemical synthesis of chemically stable isoreticular covalent organic frameworks. J. Am. Chem. Soc. *135*, 5328–5331.

53. Akkermans, R.L., Spenley, N.A., and Robertson, S.H. (2013). Monte Carlo methods in materials studio. Mol. Simulat. *39*, 1153–1164.

54. Uribe-Romo, F.J., Doonan, C.J., Furukawa, H., Oisaki, K., and Yaghi, O.M. (2011). Crystalline covalent organic frameworks with hydrazone linkages. J. Am. Chem. Soc. *133*, 11478–11481.

55. Bunck, D.N., and Dichtel, W.R. (2013). Bulk synthesis of exfoliated two-dimensional polymers using hydrazone-linked covalent organic frameworks. J. Am. Chem. Soc. *135*, 14952–14955.

56. Ding, S.Y., Dong, M., Wang, Y.W., Chen, Y.T., Wang, H.Z., Su, C.Y., and Wang, W. (2016). Thioether-based fluorescent covalent organic framework for selective detection and facile removal of mercury(II). J. Am. Chem. Soc. *138*, 3031–3037.

57. Yuan, Y., Niu, B., Yu, Q., Guo, X., Guo, Z., Wen, J., et al. (2020). Photoinduced multiple effects to enhance uranium extraction from natural seawater by black phosphorus nanosheets. Angew. Chem. Int. Ed. *59*, 1220–1227.

58. Clark, T., Chandrasekhar, J., Spitznagel, G.W., and Schleyer, P.V.R. (1983). Efficient diffuse function- augmented basis sets for anion calculations. III.* the 3-21+G basis set for first-row elements. J. Comput. Chem. *4*, 294–301.

59. Krishnan, R., Binkley, J.S., Seeger, R., and Pople, J.A. (1980). Self-consistent molecular orbital methods. XX. A basis set for correlated wave functions. J. Chem. Phys. *72*, 650–654.

60. Cao, X., Dolg, M., and Stoll, H. (2003). Valence basis sets for relativistic energy-consistent small-core actinide pseudopotentials. J. Chem. Phys. *118*, 487–496.

61. Cao, X., and Dolg, M. (2004). Segmented contraction scheme for small-core actinide pseudopotential basis sets. J. Mol. Struct.: THEOCHEM *673*, 203–209.

62. Hehre, W.J., Ditchfield, R., and Pople, J.A. (1972). Self—consistent molecular orbital methods. XII. further extensions of Gaussian—type basis sets for use in molecular orbital studies of organic molecules. J. Chem. Phys. *56*, 2257–2261.

63. Küchle, W., Dolg, M., Stoll, H., and Preuss, H. (1994). Energy-adjusted pseudopotentials for the actinides. Parameter sets and test calculations for thorium and thorium monoxide. J. Chem. Phys. *100*, 7535–7542.

64. Hariharan, P.C., and Pople, J.A. (1973). The influence of polarization functions on molecular orbital hydrogenation energies. Theoret. Chim. Acta *28*, 213–222.

65. Wang, Y., Hu, S.-X., Cheng, L., Liang, C., Yin, X., Zhang, H., Li, A., Sheng, D., Diwu, J., Wang, X., et al. (2020). Stabilization of plutonium(V) within a crown ether inclusion complex. CCS Chem. *2*, 425–431.

66. Chen, B., Hong, S., Dai, X., Li, X., Huang, Q., Sun, T., Cao, D., Zhang, H., Chai, Z., Diwu, J., and Wang, S. (2022). In vivo uranium decorporation by a tailor-made hexadentate ligand. J. Am. Chem. Soc. *144*, 11054–11058.

67. Wang, X., Dai, X., Shi, C., Wan, J., Silver, M.A., Zhang, L., Chen, L., Yi, X., Chen, B., Zhang, D., et al. (2019). A 3, 2-hydroxypyridinone-based decorporation agent that removes uranium from bones in vivo. Nat. Commun. *10*, 2570.